Chemical Sensors

Deutsche Ausgabe: DOI: 10.1002/ange.201608813
Internationale Ausgabe: DOI: 10.1002/anie.201608813

Non-Porous Iron(II)-Based Sensor: Crystallographic Insights into a Cycle of Colorful Guest-Induced Topotactic Transformations

*Santiago Rodríguez-Jiménez, Humphrey L. C. Feltham, and Sally Brooker**

Dedicated to Professor Leonard F. Lindoy on the occasion of his 80th birthday and to María Trujillo Salmerón

Abstract: *Materials capable of sensing volatile guests at room temperature by an easily monitored set of outputs are of great appeal for development as chemical sensors of small volatile organics and toxic gases. Herein the dinuclear iron(II) complex, $[Fe^{II}_2(\mathbf{L})_2(CH_3CN)_4](BF_4)_4{\cdot}2\,CH_3CN$ (**1**) [**L** = 4-(4-methylphenyl)-3-(3-pyridazinyl)-5-pyridyl-4H-1,2,4-triazole], is shown to undergo reversible single-crystal-to-single-crystal (SCSC) transformations upon exposure to vapors of different guests: **1** (MeCN)⇌**2** (EtOH)→**3** (H_2O)⇌**1** (MeCN). Whilst **1** and **2** remain dimetallic, SCSC to **3** involves conversion to a 1D polymeric chain (due to a change in **L** bridging mode), which, remarkably, can undergo SCSC de-polymerization, reforming dimetallic **1**. Additionally, SC-XRD studies of two ordered transient forms, **1TF3** and **2TF3**, confirm that guest exchange occurs by diffusion of the new guests into the non-porous lattices as the old guests leave. These reversible SCSC events also induce color and magnetic responses. Indeed dark red **1** is spin crossover active ($T_{1/2}\downarrow$ 356 K; $T_{1/2}\uparrow$ 369 K), whilst orange **2** and yellow **3** remain high spin.*

Robust porous metal–organic frameworks (MOFs)[1] are a major class of material that can admit, often selectively, small volatile organics or toxic gases, opening up many applications from sensors[2] to greenhouse gas capture,[3] gas storage,[4] increasing the octane rating of fuel,[5] and controlled catalysis.[6] Most of these applications involve guest exchange reactions[7] that take advantage of the robust polymeric network of the MOF. Interestingly, guest exchange is also possible in non-porous solids, where it occurs by diffusion through the crystal lattice, and involves either formation/cleavage of M–L bonds[8] or other reorganization (e.g. conformational) to accommodate the guest.[9]

When guest exchange occurs in single crystals without disrupting the crystallographic order, it is a single-crystal-to-single-crystal (SCSC) transformation. Molecular materials that undergo such transformations are relatively scarce,[8c–f,9,10] due to the intrinsically larger challenge of maintaining crystallographic cohesion in a molecular, not polymeric, solid. Hence careful design ("crystal engineering")[11] is required in order to access robust and flexible molecular systems that will not be damaged during cycles of uptake/release of guests.

Applications similar to those of MOFs have been realized by molecular systems, including catalytic hydrogenation[8e] guest sequestration,[10a] chemical sensing,[8d,12] molecular electronics[9a,10b,13] and opto-electronics.[8c] For chemo-sensor applications ideally the material should also have easily monitored readout options.[14] In that regard, spin crossover (SCO) complexes[15] are excellent candidates, as on application of an external stimulus, such as temperature or pressure variation, light irradiation, or the gain/loss of guest molecules, they can reversibly switch between high-spin (HS) and low-spin (LS) electronic states. Importantly, the HS and LS states usually have very different colors, molecular vibrations, M–L bond lengths, and magnetic responses, so there are multiple options for easy readout. Crystalline molecular SCO materials are highly sensitive to guest molecule exchange.[9,10b,16]

Herein we report a robust non-porous SCO-active dinuclear iron(II) complex, $[Fe_2(\mathbf{L})_2(MeCN)_4](BF_4)_4{\cdot}2MeCN$ (**1**), that undergoes reversible SCSC transformations on exposure to a variety of solvent vapors, with the associated color changes providing easy readout of the identity of the bound guest. 1,2,4-Triazole-type ligands, like **L** (Scheme 1),

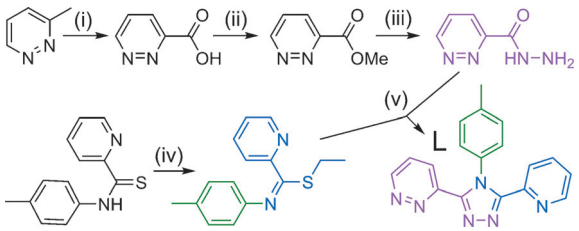

Scheme 1. Synthesis of the new ligand **L** which features pyridazine (pink), toluene (green) and pyridine (blue) substituents at the 3, 4 and 5 positions of the 1,2,4-triazole. i) SeO_2, pyridine, water; ii) $SOCl_2$, MeOH; iii) $NH_2NH_2{\cdot}H_2O$, EtOH; iv) NaOEt, EtBr; v) BuOH, 5 d reflux.

are known to be very suitable for the production of SCO active iron(II) materials.[17] Functionalization at the 3- and 5-positions by pyridazine and pyridine moieties was carried out in order to facilitate (via favorable intramolecular CH···N; Figures S7 and S12 in the Supporting Information, SI) the formation of dimetallic complexes. A tolyl substituent was employed at the 4-position as the use of that substituent on a related ligand facilitated the first quantitative guest sensor based on SCO.[12b] All of these aromatic rings in this new ligand, **L**, also contribute to a rich intermolecular network of

[*] S. Rodríguez-Jiménez, Dr. H. L. C. Feltham, Prof. S. Brooker
Department of Chemistry and MacDiarmid Institute for Advanced Materials and Nanotechnology, University of Otago
PO Box 56, Dunedin 9054 (New Zealand)
E-mail: sbrooker@chemistry.otago.ac.nz

Supporting information for this article can be found under: http://dx.doi.org/10.1002/anie.201608813.

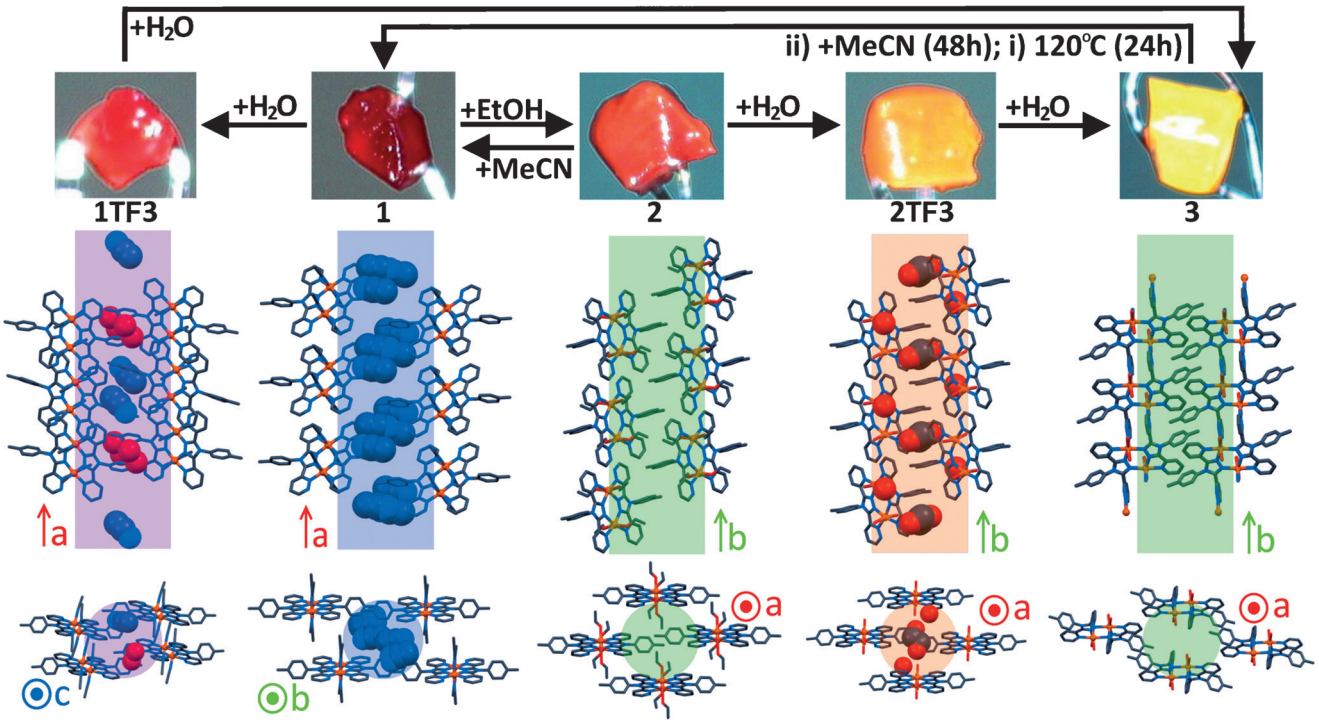

Figure 1. Summary of the observed cycle of transformations of **1**. Top: photos of single crystals (note: different single crystals were used for each data collection) of dinuclear complexes: dark red $[Fe^{II}_2(\mathbf{L})_2(MeCN)_4]$ $(BF_4)_4{\cdot}2\,MeCN$ (**1**), light red $[Fe^{II}_2(\mathbf{L})_2(MeCN)_4](BF_4)_4{\cdot}0.5\,MeCN{\cdot}0.5\,H_2O$ (**1TF3**), orange $[Fe^{II}_2(\mathbf{L})_2(EtOH)_4](BF_4)_4$ (**2**), light orange $[Fe^{II}_2(\mathbf{L})_2(H_2O)_4](BF_4)_4{\cdot}2\,H_2O{\cdot}0.5\,EtOH$ (**2TF3**), and yellow polymeric$\{[Fe^{II}_2(\mathbf{L})_2(H_2O)_4](BF_4)_4\}_\infty$ (**3**). Middle and bottom: two views of two columns of cations (three staggered π–π stacked cations shown in each column) in each of the crystal lattices, viewed: (middle) along and (bottom) down the highlighted column (located between tolyl rings of cations) of anions and/or lattice solvents (solvents, if present, shown in spacefill). Cations in wireframe; H and anions omitted for clarity. No lattice solvent in **2** and **3**; MeCN in **1**; MeCN and H_2O in **1TF3**; EtOH and H_2O in **2TF3**.

π–π contacts (see SI). These design features work together to enable production of millimeter-size single-crystals of dinuclear molecules of **1**, in a robust yet flexible crystal lattice.

Exposure of dark red crystals of dinuclear $[Fe_2(\mathbf{L})_2(MeCN)_4](BF_4)_4{\cdot}2\,MeCN$ (**1**) to ethanol vapor causes rapid SCSC conversion to orange crystals of $[Fe_2(\mathbf{L})_2(EtOH)_4](BF_4)_4$ (**2**), both of which have been structurally characterized (Figures 1, 2 and S14). This is reversible: exposure of **2** to acetonitrile vapor reforms **1** (Figure 1). Interestingly, when crystals of **1** or **2** are instead exposed to water vapor, both undergo another SCSC transformation, producing yellow crystals of polymeric $\{[Fe_2(\mathbf{L})_2(H_2O)_4](BF_4)_4\}_\infty$ (**3**) (Figures 1, 2 and S27). Furthermore, crystals of dinuclear **1** can be recovered from polymeric **3** by annealing crystals of **3** at 120 °C then re-exposing them to MeCN vapor (see below). The rate of guest exchange (Figure S37) is related to the crystal size, with larger crystals taking longer to transform completely, presumably due to slower guest diffusion into the interior of the larger crystal, through the non-porous lattice. The associated changes in color (dark red vs. orange vs. yellow), bonding (dinuclear vs. polymeric) and magnetic responses (spin crossover active versus fully high spin, see later) are dramatic, yet crystallinity is retained during **1** (MeCN)⇌**2** (EtOH)→**3** (H_2O)⇌**1** (MeCN).

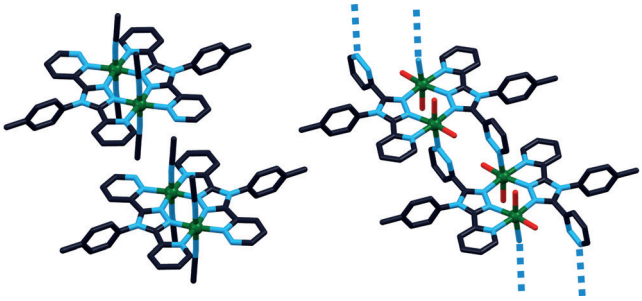

Figure 2. Representation emphasizing the dramatic transformation between the discrete dinuclear **1** with *trans*-MeCN co-ligands (left) and the polymeric **3** with *cis*-H_2O co-ligands (right), upon water vapor exposure. Fe (green), N (blue), O (red), C (black).

Two ordered transient forms,[18] between **1** and **3**, $[Fe^{II}_2(\mathbf{L})_2(MeCN)_4](BF_4)_4{\cdot}0.5\,MeCN{\cdot}0.5\,H_2O$ (**1TF3**), and between **2** and **3**, $[Fe^{II}_2(\mathbf{L})_2(H_2O)_4](BF_4)_4{\cdot}2\,H_2O{\cdot}0.5\,EtOH$ (**2TF3**) were captured and also characterized by single-crystal X-ray diffraction (SC-XRD), in house (Figures 1, S9–S12 and S18–S22).

All five of the structures are in the triclinic space group $P\bar{1}$ (Table 1), with half of a dinuclear complex in the asymmetric unit (two halves in the case of **1TF3**) and inversion generating the other half, and six coordinate iron(II) centers (Figure 1). The octahedral distortion parameter Σ ranges widely, from 50 to 112° (Table 1). At 100 K, the Fe–donor bond lengths (1.954–1.961 Å) are consistent[15a] with [LS-LS] for N_6-coordinated **1** and **1TF3**, whereas N_4O_2-coordinated **2**, **2TF3**, and **3** (2.153–2.161 Å) are fully HS (Tables 1 and S3).

Table 1: Selected crystallographic data for all five structures. All in the triclinic space group $P\bar{1}$, and at 100 K (except **3** at 90 K): $[Fe^{II}_2(\mathbf{L})_2(MeCN)_4](BF_4)_4 \cdot 2\,MeCN$ (**1**), $[Fe^{II}_2(\mathbf{L})_2(MeCN)_4](BF_4)_4 \cdot 0.5\,MeCN \cdot 0.5\,H_2O$ (**1TF3**), $[Fe^{II}_2(\mathbf{L})_2(EtOH)_4](BF_4)_4$ (**2**), $[Fe^{II}_2(\mathbf{L})_2(H_2O)_4](BF_4)_4 \cdot 2\,H_2O \cdot 0.5\,EtOH$ (**2TF3**) and $\{[Fe_2(\mathbf{L})_2(H_2O)_4](BF_4)_4\}_\infty$ (**3**).

	1	1TF3	2	2TF3	3
Solv. cryst./Fe_2	2 MeCN	0.5 MeCN and 0.5 H_2O	None	0.5 EtOH and 2 H_2O	None
M_r	1333.97	1281.4	1271.91	1218.77	1159.7
V [Å^3]; Z	1534.38(5); $Z=1$	2759.1(8); $Z=2$	1318.13(2); $Z=1$	1274.0(5); $Z=1$	1085.61(14); $Z=1$
ρ_{calcd} [Mg m^3]	1.444	1.542	1.602	1.589	1.774
R1/wR2	0.0562/0.1751	0.1486/0.3413	0.0777/0.2007	0.1149/0.2654	0.0473/0.1271
Av. Fe–donor [Å]	1.954	1.961/ 1.960[a]	2.158	2.153	2.161
Fe donor set	N_6	N_6	N_4O_2	N_4O_2	N_4O_2
Σ [°][b]	52.14	52.20/ 55.60[a]	111.37	97.8	50.04
Triaz vs. Pdz [°][c]	3.52	1.59/ 5.35[a]	2.34	3.07	86.21
Triaz vs. Pyr [°][d]	5.51	7.94/ 7.06[a]	4.97	3.11	12.30
Tolyl twist [°][e]	79.72	62.91/ 66.29, 89.04[f]	78.46	85.14	88.54

[a] **1TF3** contains two independent iron centers. [b] Octahedral distortion parameter, Σ, is the sum of the deviations from 90° of the 12 *cis* angles in the coordination sphere.[19] [c] Angle between the mean planes of the triazole ring and attached pyridazinyl ring. [d] Angle between the mean planes of the triazole ring and attached pyridyl ring. [e] Angle between the mean planes of the triazole ring and attached tolyl ring. [f] **1TF3** contains two independent iron centers, Fe1 and Fe2. For Fe2 the coordinated **L** has a 50:50 disordered tolyl ring (Figures S9 and S10).

In all four dinuclear complexes the two iron(II) centers are sandwiched by two bis-bidentate **L** ligands which provide a fairly flat equatorial plane and two triazole bridges between them (see Figure 1, Table 1, SI). The coordination of each iron(II) center is completed by a pair of *trans* (axial) donors: MeCN for **1** and **1TF3**, EtOH for **2**, and H_2O for **2TF3**.

For the polymeric complex, **3**, whilst the pyridine pocket binds as before and the triazole bridges to the second iron(II) center, the pyridazine pocket of **L** is very differently coordinated. The pyridazine is twisted right away (86.21° to triazole) in order to bind in a monodentate fashion to an iron(II) center in the next complex, generating a polymeric chain (Figures 1, 2 and S27). The N_4O_2 coordination is completed by *cis* coordination of two H_2O molecules. Remarkably, these major changes, which convert what was a discrete dinuclear complex into a polymer, also occur without destruction of the crystal—and they are reversible: SCSC de-polymerization reforms **1**.

The supramolecular array of π–π, CH···π, anion···π and H-bonding found in **1** organizes the cations into a staggered stack (Figures 1 and S8). This is maintained throughout these SCSC transformations (Figures 1, S11, S15, and S20), although for polymeric **3** the SCSC transformation from discrete to polymeric, by Fe–N(pyridazine) bond cleavage/formation, causes changes to the details (Figures 1, 2 and S27). Interestingly, all of these transformations occur in an SCSC (i.e. topotactic[20]) manner, with the cations remaining stacked in columns, between which the BF_4^- anions/lattice solvent are accommodated (Figure 1, colour shaded regions). Lattice solvent is only present in three cases (**1**, **1TF3** and **2TF3**) and is located in between the tolyl rings of **L** in the columns of stacked cations (Figure 1; where lattice solvent is disordered, both positions are shown).

There are no voids in any of these structures so guest exchange must be by diffusion through the non-porous lattices. This mostly occurs in an associative manner, with new guests entering as the old guests leave, as both types of guest are present in the transient form structures of **1TF3** and **2TF3**. This non-disruptive dynamic process may be aided by rotation of the tolyl rings with respect to the triazole (Table 1) to facilitate guest diffusion. The tolyl rings also play an important role in the packing, fine-tuning the spacing between cations, which may also enhance the guest diffusion, and subsequent accommodation of the guests as well as the anions, whilst maintaining the integrity of the crystal (Figure 1).

Whilst of modest quality, the structure determinations of the ordered transient forms **1TF3** and **2TF3** provide important crystallographic insights. Specifically, **1TF3** still shares several features with **1**, including MeCN bound LS iron(II) dinuclear complexes. But instead of only disordered MeCN molecules of solvation located in between the tolyl rings (as in **1**), now there is a mixture of H_2O and MeCN present, so some MeCN has departed and some H_2O has entered. This snapshot indicates that the H_2O is diffusing into the lattice, perhaps aided by rotation of the tolyl rings (as noted above), so that in the next stage it can coordinate in place of the MeCN, to give H_2O coordinated HS **3**. Similarly, **2TF3** remains HS dinuclear iron(II) like in **2**, but it already shares several features with **3**, including H_2O bound to the HS iron(II) centers, albeit *trans* to one another, prior to polymerization to form *cis*-H_2O coordinated polymer **3**. Unlike both **2** and **3**, **2TF3** contains lattice solvent, specifically the departing EtOH and excess H_2O molecules: these are lost on polymerization to form **3**, the most dense of these compounds (Figure S2). In summary, these snapshots indicate that during these SCSC transformations the diffusion of new guests into the non-porous crystal lattice occurs as the old guests leave (Figure 1, Table 1).

The density increases on SCSC transformation from **1** (MeCN)→**2** (EtOH)→**3** (H_2O), from 1.444 to 1.602 to 1.774 Mg m^3 (Table 1). Polymer **3** has the highest density, and de-polymerization of **3** is the only SCSC transformation described herein to require a drying step before introduction of the new guest.

Powder X-ray diffraction (PXRD) revealed distinctive peaks for **1** at 5.90°, for **2** at 8.32°, and for **3** at 7.08°. These matched those calculated from the SC-XRD data (Figure 3,

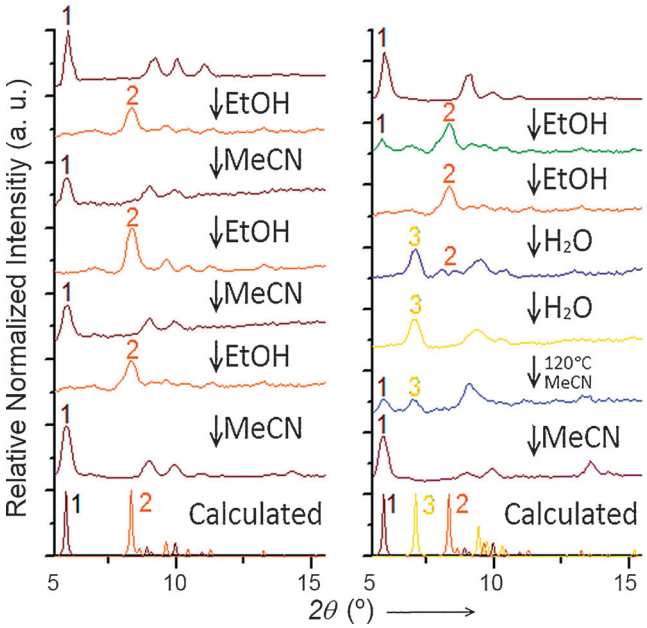

Figure 3. Sequence of PXRD plots showing (left) three cycles of the reversible SCSC conversions of **1** (maroon trace; main peak: 5.90°)⇌**2** (orange trace, main peak: 8.32°), on exposure to either EtOH or MeOH vapor, as appropriate. (Right) cycle of SCSC transformations starting from **1** (top, maroon trace) to **2** (orange trace) to **3** (yellow trace) and back to **1** [carried out by exposure to EtOH, then H_2O, vapor; then annealing **3** at 120 °C for 24 h before exposure to MeCN vapor for 24 h (blue trace), with conversion complete after 48 h total exposure to MeCN vapor (bottom, maroon trace)]. The PXRD spectra calculated from the SC-XRD data for **1**–**3** are shown at the bottom, and are a good match for the observed spectra.

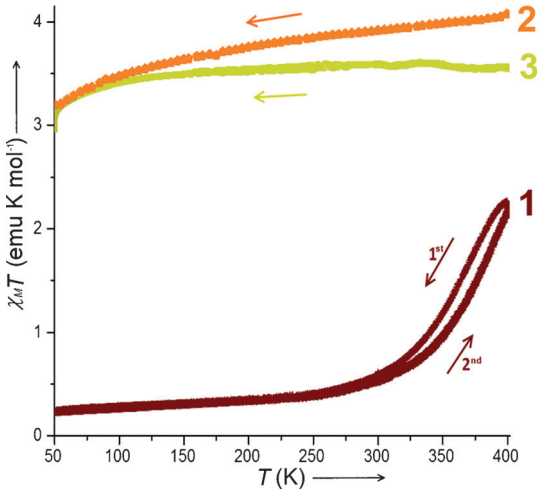

Figure 4. $\chi_M T$ (per Fe) versus T (sweep mode at 2 K min^{-1}) for **1** (maroon trace; 400–450-400 K), **2** (orange trace), and **3** (yellow trace).

bottom, Figures S29–S32). PXRD was therefore able to monitor guest-exchange activity. Three cycles of dark red **1**⇌orange **2** SCSC transformations were completed (Figure 3, left). Similarly, a **1**→**2**→**3**→**1** cycle of SCSC transformations, which includes polymerization, **2**→**3**, and de-polymerization, **3**→**1**, was successfully completed (Figure 3, right).

These solid-state SCSC transformations, **1**⇌**2**→**3**⇌**1**, can also be followed by eye, due to the characteristic dark red⇌orange→yellow⇌dark red colors (Figure 1).

Dark red **1** was magnetically characterized in a sealed capsule to prevent solvent loss during the measurements. It remains [LS-LS] at room temperature, but undergoes a gradual SCO when heated to 400 K, with $\chi_M T$ (per Fe) reaching 2.45 emu K mol^{-1}, corresponding to about 80 % [HS-HS].[15a] On cooling it exhibits a narrow hysteresis loop of 13 K ($T_{1/2}\downarrow$ = 356 K; $T_{1/2}\uparrow$ = 369 K, Figure 4), a loop that is retained over at least 8 warming–cooling cycles (Figures S33 and S34). In contrast, orange **2** and yellow **3** remain HS (consistent with SC-XRD at 100 and 90 K, respectively).

In summary, these detailed crystallographic investigations, especially of the two ordered transient forms, improve our understanding of how SCSC transformations occur in non-porous molecular solids like **1**. Here the non-destructive guest exchange processes mostly occur associatively, with new guests coming in at the same time as the old guests leave. The alternative, dissociative, that is, loss of the old guest followed by new guest uptake, is seen only for the de-polymerization of **3**.

Remarkably, **1** exhibits reversible SCSC guest molecule exchange while producing a set of red, orange or yellow readouts, signalling which of MeCN, EtOH or H_2O guests, respectively, have been taken up. These findings demonstrate that such systems—non-porous molecular systems—have great potential as chemical sensors for a range of volatile guests.

Acknowledgements

We thank the University of Otago (including award of a PhD scholarship to S.R.J. and the 2015 purchase of a Versalab magnetometer which enabled in house 50–400 K magnetic measurements) and the Marsden Fund (RSNZ; including a research fellowship to H.L.C.F.) for supporting this research. We are grateful to Professors Peter J. Steel (Canterbury) and Geoffrey B. Jameson (Massey) for helpful discussions, and thank Lisa Bucke (Otago) for help with the TOC.

Keywords: chemical sensor · crystal engineering · reversible guest exchange · single-crystal-to-single-crystal transformation · spin crossover

How to cite: *Angew. Chem. Int. Ed.* **2016**, *55*, 15067–15071
Angew. Chem. **2016**, *128*, 15291–15295

[1] a) S. R. Batten, R. Robson, *Angew. Chem. Int. Ed.* **1998**, *37*, 1460–1494; *Angew. Chem.* **1998**, *110*, 1558–1595; b) M. Eddaoudi, D. B. Moler, H. Li, B. Chen, T. M. Reineke, M. O'Keefe, O. M. Yaghi, *Acc. Chem. Res.* **2001**, *34*, 319–330.

[2] a) G. J. Halder, C. J. Kepert, B. Moubaraki, K. S. Murray, C. S. Cashion, *Science* **2002**, *298*, 1762–1765; b) A. Galet, A. B. Gaspar, M. C. Muñoz, G. V. Bukin, G. Levchenko, J. A. Real, *Adv. Mater.* **2005**, *17*, 2949–2953; c) P. D. Southon, L. Llu, E. A. Fellows, D. J. Price, G. J. Halder, K. W. Chapman, B. Moubaraki,

K. S. Murray, J.-F. Létard, C. J. Kepert, *J. Am. Chem. Soc.* **2009**, *131*, 10998 – 11009; d) R. Ohtani, K. Yoneda, S. Furukawa, N. Horike, S. Kitagawa, A. B. Gaspar, M. C. Muñoz, J. A. Real, M. Ohba, *J. Am. Chem. Soc.* **2011**, *133*, 8600 – 8605; e) E. Coronado, G. Minguez Espallargas, *Chem. Soc. Rev.* **2013**, *42*, 1525 – 1539.

[3] a) K. Sumida, D. L. Rogow, J. A. Mason, T. M. McDonald, E. D. Bloch, Z. R. Herm, T.-H. Bae, J. R. Long, *Chem. Rev.* **2012**, *112*, 724 – 781; b) M. G. Cowan, R. G. Miller, P. D. Southon, J. R. Price, O. Yazaydin, J. R. Lane, C. J. Kepert, S. Brooker, *Inorg. Chem.* **2014**, *53*, 12076 – 12224, and front cover.

[4] a) A. R. Millward, O. M. Yaghi, *J. Am. Chem. Soc.* **2005**, *127*, 17998 – 17999; b) J. Mason, M. Veenstra, J. R. Long, *Chem. Sci.* **2014**, *5*, 32 – 51.

[5] Z. R. Herm, E. D. Bloch, J. R. Long, *Chem. Mater.* **2014**, *26*, 323 – 338.

[6] M. I. Gonzalez, E. D. Bloch, J. A. Mason, S. J. Teat, J. R. Long, *Inorg. Chem.* **2015**, *54*, 2995 – 3005.

[7] a) J. Lee, O. K. Farha, J. Roberts, K. A. Scheidt, S. T. Nguyen, J. T. Hupp, *Chem. Soc. Rev.* **2009**, *38*, 1450 – 1459; b) H. Kitagawa, *Nat. Chem.* **2009**, *1*, 689 – 690; c) L. E. Kreno, K. Leong, O. K. Farha, M. Allendorf, R. P. Van Duyne, J. T. Hupp, *Chem. Rev.* **2012**, *112*, 1105 – 1125.

[8] a) E. Coronado, M. Gimenez-Marques, G. M. Espallargas, L. Brammer, *Nat. Commun.* **2012**, *3*, 828; b) A. Lennartson, P. Southon, N. F. Sciortino, C. J. Kepert, C. Frandsen, S. Mørup, S. Piligkos, C. J. McKenzie, *Chem. Eur. J.* **2015**, *21*, 16066 – 16072; c) M. Albrecht, M. Lutz, A. L. Spek, G. van Koten, *Nature* **2000**, *406*, 970 – 974; d) S. Supriya, S. K. Das, *J. Am. Chem. Soc.* **2007**, *129*, 3464 – 3465; e) Z. Huang, P. S. White, M. Brookhart, *Nature* **2010**, *465*, 598 – 601; f) J. Sundberg, L. J. Cameron, P. D. Southon, C. J. Kepert, C. J. McKenzie, *Chem. Sci.* **2014**, *5*, 4017 – 4025.

[9] a) R.-J. Wei, Q. Huo, J. Tao, R.-B. Huang, L.-S. Zheng, *Angew. Chem. Int. Ed.* **2011**, *50*, 8940 – 8943; *Angew. Chem.* **2011**, *123*, 9102 – 9105; b) J. S. Costa, S. Rodríguez-Jiménez, G. A. Craig, B. Barth, C. M. Beavers, S. J. Teat, G. Aromí, *J. Am. Chem. Soc.* **2014**, *136*, 3869 – 3874.

[10] a) J. L. Atwood, L. J. Barbour, A. Jerga, B. L. Schottel, *Science* **2002**, *298*, 1000 – 1002; b) B. Li, R.-J. Wei, J. Tao, R.-B. Huang, L.-S. Zheng, Z. Zheng, *J. Am. Chem. Soc.* **2010**, *132*, 1558 – 1566.

[11] G. R. Desiraju, *Angew. Chem. Int. Ed.* **2007**, *46*, 8342 – 8356; *Angew. Chem.* **2007**, *119*, 8492 – 8508.

[12] a) S. Sabbani, S. K. Das, *CrystEngComm* **2015**, *17*, 8850 – 8857; b) R. G. Miller, S. Brooker, *Chem. Sci.* **2016**, *7*, 2501 – 2505, and front cover feature.

[13] M. Nihei, L. Han, H. Oshio, *J. Am. Chem. Soc.* **2007**, *129*, 5312 – 5313.

[14] O. S. Wenger, *Chem. Rev.* **2013**, *113*, 3686 – 3733.

[15] a) P. Gütlich, H. A. Goodwin, *Top. Curr. Chem.* **2004**, *233 – 235*; b) A. Bousseksou, G. Molnar, L. Salmon, W. Nicolazzi, *Chem. Soc. Rev.* **2011**, *40*, 3313 – 3335; c) T. Matsumoto, G. N. Newton, T. Shiga, S. Hayami, Y. Matsui, H. Okamoto, R. Kumai, Y. Murakami, H. Oshio, *Nat. Commun.* **2014**, *5*, 3865; d) S. Brooker, *Chem. Soc. Rev.* **2015**, *44*, 2880 – 2892, and front cover feature.

[16] a) R.-J. Wei, J. Tao, R.-B. Huang, L.-S. Zheng, *Inorg. Chem.* **2011**, *50*, 8553 – 8564; b) E. Coronado, M. Giménez-Marqués, G. Mínguez Espallargas, F. Rey, I. J. Vitórica-Yrezábal, *J. Am. Chem. Soc.* **2013**, *135*, 15986 – 15989.

[17] a) O. Kahn, E. Codjovi, *Philos. Trans. R. Soc. London Ser. A* **1996**, *354*, 359 – 379; b) J. G. Haasnoot, *1,2,4-Triazoles as Ligands for Iron(II) High Spin-Low Spin Crossovers*, Kluwer, Dordrecht, **1996**; c) J. A. Kitchen, S. Brooker, *Coord. Chem. Rev.* **2008**, *252*, 2072 – 2092; d) G. Aromí, L. A. Barrios, O. Roubeau, P. Gamez, *Coord. Chem. Rev.* **2011**, *255*, 485 – 546.

[18] G. Aromí, C. M. Beavers, J. Sanchez Costa, G. A. Craig, G. Minguez Espallargas, A. Orera, O. Roubeau, *Chem. Sci.* **2016**, *7*, 2907 – 2915.

[19] a) F. A. Deeney, J. H. Charles, G. G. Morgan, V. McKee, J. Nelson, S. J. Teat, W. Clegg, *J. Chem. Soc. Dalton Trans.* **1998**, 1837 – 1843; b) P. Guionneau, C. Brigouleix, Y. Barrans, A. E. Goeta, J.-F. Létard, J. A. K. Howard, J. Gaultier, D. Chasseau, *C. R. Acad. Sci. Ser. IIc* **2001**, *4*, 161 – 171.

[20] G. B. Jameson, H. R. Oswald, H. R. Beer, *J. Am. Chem. Soc.* **1984**, *106*, 1669 – 1675.

Received: September 8, 2016
Published online: October 12, 2016

